IL NUOVO CIMENTO Vol. 31 C, N. 5-6 Settembre-Dicembre 2008
DOI 10.1393/ncc/i2009-10345-4

Induced structures under seasonal flow conditions in the Ebro delta shelf. Laboratory and numerical models

J. A. Carrillo(1), J. M. Redondo(1), P. Fraunie(2) and N. Durand(3)

(1) *Department of Applied Physics - U.P.C. Campus Nord, Barcelona 08034 Spain*
(2) *Université de Toulon et du Var - BP 132 La Garde Cedex, France*
(3) *BRGM-SGR/LRO - Montpelier 34000, France*

(ricevuto il 10 Dicembre 2008; approvato il 10 Marzo 2009; pubblicato online il 22 Giugno 2009)

Summary. — The characteristic induced length scale produced by a river flow in its outlet is studied. Two experimental methods are compared: a) Physical modeling in laboratory and b) numerical mesoscale diffusion model; under low tidal and realistic seasonal flow conditions from Spring, Summer, Fall and Winter field data from the Ebro delta shelf. The physical laboratory experiences were performed on a five-meter diameter turntable, using the Froude-Rossby similarity. This paper shows complementary results from both methods investigating the vortex characteristic and the dynamics of the flow. The experimental results under rotating conditions show coherent vortex dynamics in the large-meso scale coastal boundary. The numerical model, on the other hand, lacks the mesoscale vortex dynamics and its induced diffusion but gives reasonable flow conditions in the close region (15–20 km) around the river mouth. Both the experiments and numerical simulations show river plume diffusion smaller than $D^2 \propto t^3$.

PACS 92.60.-e – Properties and dynamics of the atmosphere; meteorology.
PACS 92.60.Fm – Boundary layer structure and processes.
PACS 92.60.Gn – Winds and their effects.

1. – Introduction

The littoral area has had an extensive use by mankind, where developments and economic activities such as tourism, industries and harbor sites take place. Additionally the fresh water and land uses upstream of rivers have strong effects on the near marine zones. Areas like the Ebro delta river mouth in the North Western Mediterranean are dynamically complex and have been studied lately under the mesoscale perspective. The studied area is denominated the Region of Freshwater Influence (ROFI) [1,2], and needs to be modeled taking into account a large range of scales in order to make realistic predictions [3].

The study of the dispersion and dilution of the buoyant river plume in a river mouth like the Ebro is necessary to understand the plume dynamic as its exerts a large influence over the primary biological productivity in the zone. Moreover, the pollutants such as pesticides, tensioactives, heavy metals and antropogenic toxic compounds often carried by the river, also produce a large influence in the surrounding coastal area. These elements must be controlled and monitored by an array of preventive and remedial tools like *in situ* campaigns, numerical and laboratory models. Several authors have been working in the area such as [4] and [5] in field campaigns at mesoscale, [6] and [7] in field campaigns at meso and large scale, [8] and [9] in numerical approximations at mesoscale and [10] in numerical approximations at large scale, but there is often divergence between the models and the field data.

The sole applications of field campaigns are very expensive logistical and economically, the joint application of numerical and laboratory models which are much cheaper can be considered as a real practical alternative provided validation checks are carried out. Laboratory data is also a useful alternative to validate and control numerical parameters hard to measure in the environment [11]. The laboratory experiments shown at this work are just a step in an integrated study in coastal mixing that began in [12], showing the coastal distribution of coherent mesoscale eddies.

Next we present a description of the Ebro delta and its flow characteristics in sect. **2** and sect. **3**, section **5** describes the laboratory experiments used to model the river outflow plume. Section **6** presents the scaling law used and sect. **7** the numerical simulations applied; finally we present a comparison of different results and the final conclusions.

2. – Description of the studied area

The river Ebro estuary is in the occidental Mediterranean Sea. Its flow presents a strong variation from $100\,\mathrm{m^3\,s^{-1}}$ to $3200\,\mathrm{m^3\,s^{-1}}$, these seasonal flow variations are due mainly to rain and thaw in the basin. They determine the general dynamics in the estuary and in the adjacent coastal zone thanks to the river plume diffusion. The Ebro river flows into the Mediterranean and its last 32 km form a delta (fig. 1) located at the coordinates $40°40'$ N and $0°40'$ W [13,14]. An estuary is present with strong mixing processes between river and sea water with different characteristics such as salinity, temperature, nutrients and pollutants. Pritchard [15] classifies the Ebro delta estuary such as an estuary of kind II, where it implies the presence of a stable salt wedge.

3. – Mean flow

The mean flow evaluated by the Confederación Hidrográfica del Ebro [16] in the Mezquinenza dam during the period between the 1912 to 1986, shows a standard yearly cycle with maximum flow of $450\,\mathrm{m^3\,s^{-1}}$ in January-February, followed by a constant reduction towards $350\,\mathrm{m^3\,s^{-1}}$ from May to June. Falling further in July-August until the lowest flow of $100\,\mathrm{m^3\,s^{-1}}$, later between the months of September-December the flow values recover the $450\,\mathrm{m^3\,s^{-1}}$ maximum. Figure 2 represents these mean monthly values.

4. – Flow characteristics in the river mouth

As was mentioned, the estuary presence in the last portion of the river presents a change in salinity on the river waters. This salinity variation causes changes in density due to the mixing between the river body flowing at the surface and the salt wedge waters

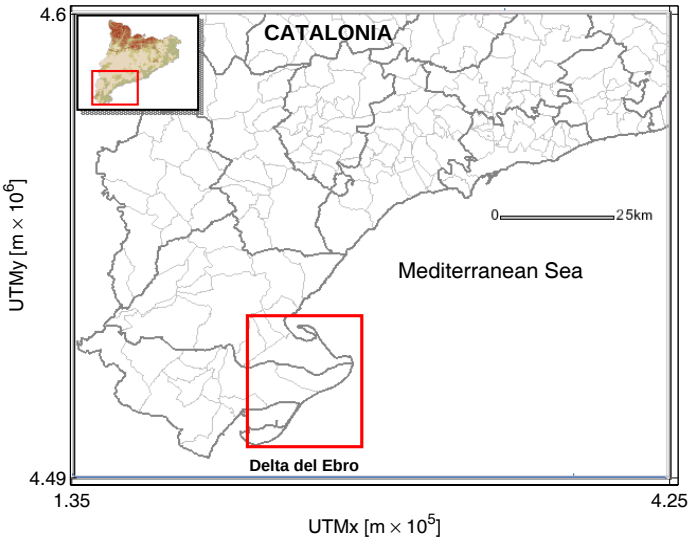

Fig. 1. – Studied area. The delta River Ebro in the NW Mediterranean Sea.

entraining upstream from the river mouth as a dense gravity current. Due to both the estuary length and the mixing dynamics that strongly depend on the river flow, the river layer salinity and its distribution in the river mouth follow quite closely the seasonal flow changes.

5. – Methods and materials

5˙1. *Laboratory experiments*. – The laboratory experiments were made in a five-meter turntable of the *SINTEF* laboratories in Trondheim, Norway. A 2×4 meters tank was placed in the center of the turntable (fig. 3). The Ebro delta shape was simplified to a geometric shape shown in fig. 4 and put at a side of the rectangular tank that modeled the area shown in fig. 5. Additionally, a wooden wall was placed to approximate the coastal shape near to the delta.

According to the real river mouth position a silicon tube was placed ($\phi = 6\,\mathrm{mm}$) at the correct place and angle. Colored freshwater with a density equal to $997\,\mathrm{kgm}^{-3}$ was pumped by means of the tube with the help of a variable flow pump. The experimental tank had salty water with a density equal to $1027\,\mathrm{kgm}^{-3}$, so it complied with the compensated buoyancy and time as described in eq. (3).

In the centre of the tank at 2 meters height a video camera was placed in order to capture the experimental images of the flow for later analysis at a frequency of 50 Hz. All the experiments were recorded in tapes with a video type recorder SVHS and the images were digitalized with the fluid dynamics visualization program *DigImage* [17, 12, 18].

5˙1.1. Experimental initial conditions. The horizontal and vertical relationships of the length scales between the natural real flow and the experimental model were $1 : 0.5 \times 10^5$ in horizontal, and $1 : 53$ in vertical. The time relationship derived in the next section implies that a day in the real Ebro delta is represented by 4.1 seconds in the experimental model. In the experiments described in this paper four flow conditions in the river mouth

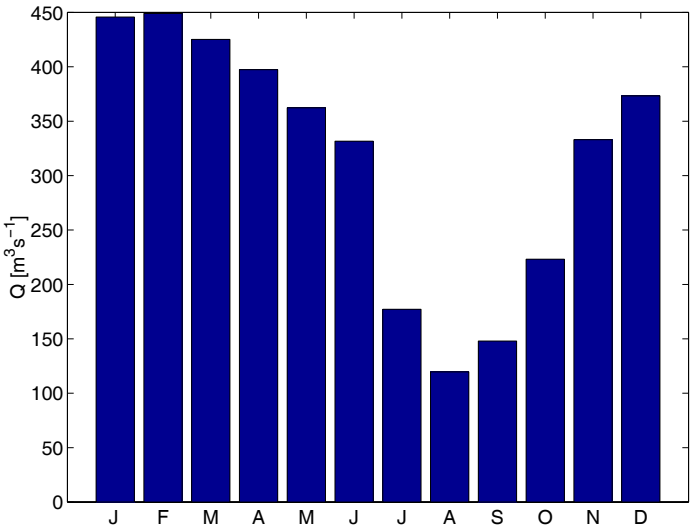

Fig. 2. – Mean river flow values from the River Ebro during the period from 1912 to 1986 from [16].

were used, in accordance with the local flow measured by [19]. The local flows 121, 114, 287 y 635 $m^3 s^{-1}$ measured in field experiments during the Spring, Summer, Fall and Winter conditions, correspond to the experimental jet velocity of 0.505, 0.280, 0.546 y 0.896 ms^{-1}, respectively.

In all the cases the temperature values were 17.4 °C to freshwater and 24.0 °C to salt water. Salinity in the same order was 39.5 y 0.0 gkg^{-1} and the rotation period

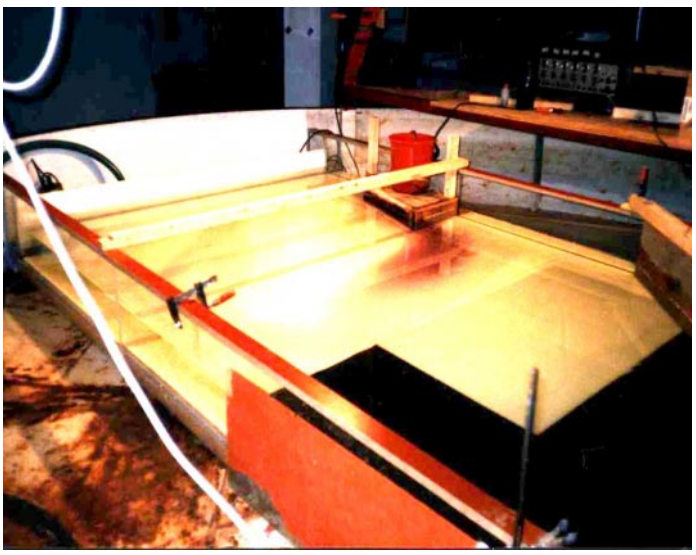

Fig. 3. – Experimental rectangular tank (4×2 m) within the five meters turntable.

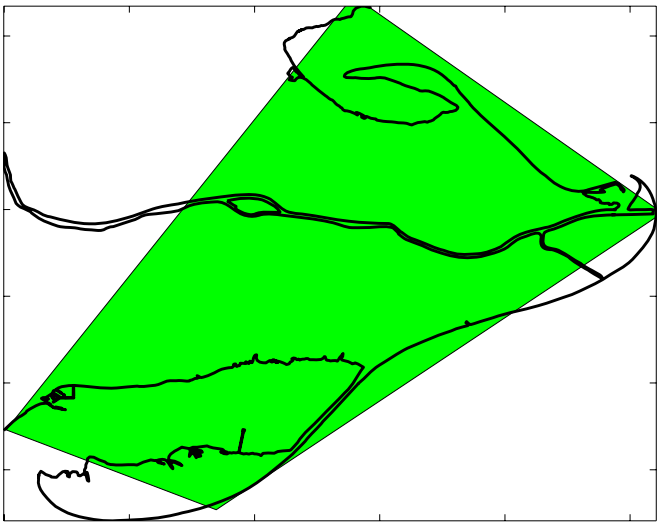

Fig. 4. – Geometric simplification from the delta del Ebro, used in the laboratory experiments.

was $51.15\,\mathrm{s}^{-1}$. The turntable was kept turning 15 minutes before each experiment so that equilibrium was reached and the flow inside the tank was stable and lost the angular acceleration inertia, since this set-up was extremely sensitive to small variations in the angular velocity, these were kept to a minimum following the procedures of [11].

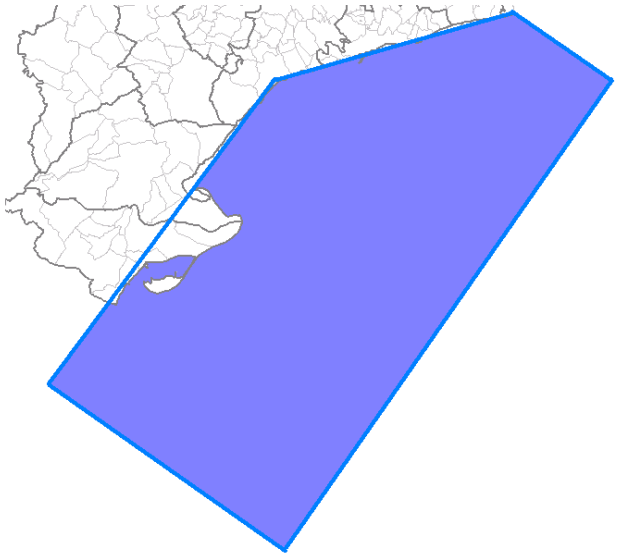

Fig. 5. – Graphic representation from the experimental studied area inside the rectangular tank.

6. – Basic equations and laboratory scaling

Three are the main characteristics in the experimental model to bear in mind with respect to the real flow. These are:

1) The horizontal and vertical scale relationships.

2) The velocity scale relationship.

3) The time scale relationship.

The horizontal and vertical scale relationships were determined by the experimental tank dimensions, and correspond to $1 : 0.5 \times 10^5$ and $1 : 53$, respectively. With regard to these scale relationships we calculated the velocity relationships using Rossby and Froude scaling for the time.

6˙1. *Froude number*. – The relevant parameter to simulate ocean currents is the densimetric Froude number. This relates the inertial forces with the gravity forces and the characteristic depth in the following way:

$$Fr = \frac{u}{(g'h)^{1/2}}\,, \tag{1}$$

where u and h are the characteristic velocity and depth g' is the compensated gravity $g' = \frac{\Delta\rho}{\rho} g$. Applying (1) to the natural (n) and experimental (e) models, the Froude number will provide the relationship

$$Fr_n = \frac{u_n}{(g'_n h_n)^{1/2}} = \frac{u_e}{(g'_e h_e)^{1/2}}\,. \tag{2}$$

Solving (2) the compensated gravity value in the experimental model must be used the time following the relationship

$$g'_e = \frac{(\frac{u_e}{Fr_n})^2}{h_e}\,. \tag{3}$$

Calculate the experimental velocities needed to fulfill (3) with the chosen density difference produced by salt solutions. This is also needed for the comparison of angular velocities in order that the general flow conditions can be compared. In this case, the mixing is driven by the shear between the river and sea layers. Because of the shear in the outflowing current, the use of the Richardson number controls mixing processes in both experimental and field conditions.

The overall or bulk Richardson number may be written as

$$Ri = \frac{g\Delta\rho\ell}{\rho(\Delta u)^2}\,. \tag{4}$$

If shear $\frac{\partial u}{\partial z} \approx \frac{\Delta u}{\ell}$ and density gradient $\frac{\partial \rho}{\partial z} \approx \frac{\Delta \rho}{\ell}$ correspond to the characteristic depth $\frac{\Delta u}{\ell} \approx \frac{u}{h}$, the Richardson number is related to the Froude number as

$$Ri = Fr^{-2}. \tag{5}$$

So that the scaling may be adjusted to model the mean flow (Fr) or the mixing caused by shear (Ri).

6˙2. *Rossby number*. – Formally, the Rossby number is defined as the relationship between the inertial forces and the rotational forces in the following way:

$$Ro = \frac{u}{fL}\,. \tag{6}$$

It may also be interpreted as the ratio between the local vorticity induced by the flow $\omega \approx \frac{u}{L}$ and the induced vorticity by external rotation f. Here the Coriolis parameter f is defined as twice the vertical component of the angular velocity ($f = 2\Omega$); u and L are the characteristic horizontal flow velocity and the length scale. If the Earth's shape is approximated to a sphere, the Coriolis parameter will be twice the Earth's angular velocity multiplied by the sine of the latitude (at the site). The expression will be then $f = 2\Omega \sin(lat)$. Using (6) to equate the natural (n) and experimental (e) Rossby values:

$$Ro_n = \frac{u_n}{f_n L_n} = \frac{u_e}{f_e L_e} \tag{7}$$

and solving (7), we may obtain the angular velocity needed for the experiments:

$$f_e = \frac{u_e}{L_e Ro_n}\,, \tag{8}$$

and eliminating the horizontal velocity between (8) and (2) we can use as a check

$$f_e L_e Ro = Fr \left(g \frac{\Delta\rho_e}{\rho} h_e \right)^{1/2}, \tag{9}$$

that leads to an expression of the Rossby radius of deformation with N, the Brunt-Väisälä frequency, if $Ro = Fr$,

$$L_{Ro} = \frac{N_e}{f_e} h_e. \tag{10}$$

6˙3. *Experimental and natural time relationship*. – The time relationship (T_r) between natural real time from the performed phenomena and the experimental time is defined by

$$T_r = \frac{T_n}{T_e}\,. \tag{11}$$

This relationship (11) can be expressed employing the densimetric Froude law from (1) according to [20]. The rate between natural and experimental models in the way:

$$T_r = \frac{L_r}{(g'_r h_r)^{1/2}}\,, \tag{12}$$

where the sub index r indicates the scale rates. L is the horizontal, h the vertical and g' the compensated gravity, in this case the rate time ($1 : 354240$) shows that a day in the real Ebro delta plume is represented by 4.1 seconds in the model.

7. – Mesoscale numerical model

The non-hydrostatic free-surface and 3D hydro-dynamical model [21, 22] adapted to the Ebro site [8] was used. The model assumes incompressibility of the fluid and f-plane hypothesis, follows Boussinesq approximation and neglects molecular diffusion. The Reynolds-averaged equations like the Navier-Stokes (13), the continuity (14) and the transport equation for salinity (15) are solved by a finite-volume method. The density variations in the Ebro plume are mainly controlled by salinity differences, no temperature evolution equation is solved herein. Spatial discretization is achieved with the centered schemes of second order excepting the advection terms for which upwind schemes are used; moreover, since the experimental model has not included wind, this effect was not reproduced. Euler scheme is used for temporal discretization.

$$\frac{\partial U_i}{\partial t} = -\frac{\partial (U_i U_j)}{\partial x_j} - \frac{\partial (\overline{u_i' u_j'})}{\partial x_j} - \frac{1}{\rho_r}\frac{\partial P_d}{\partial x_j} + (1-\delta_{i3})\left[g\frac{\partial \eta}{\partial x_i} - \frac{g}{\rho_r}\int_{\eta}^{x_3}\frac{\partial \rho}{\partial x_i}\mathrm{d}x_3'\right] + \varepsilon_{ij3} f U_j, \tag{13}$$

$$\frac{\partial U_j}{\partial x_j} = 0, \tag{14}$$

$$\frac{\partial S}{\partial t} = -\frac{\partial (U_j S)}{\partial x_j} - \frac{\partial (\overline{u_j' s'})}{\partial x_j}\,. \tag{15}$$

In order to account for mixing between the river fresh water and the environmental salty water, the equation of state (16) is solved at each time-step and the result density file is introduced in the buoyancy term of the energy equation. The evolution of the surface elevation is computed by the kinematic condition at the sea surface in (17):

$$\rho = \rho_r(1 + \beta_S(S - S_r)), \tag{16}$$

$$\frac{\partial \eta}{\partial t} = U_3|_{x_3=\eta} - U_1|_{x_3=\eta}\frac{\partial \eta}{\partial x_1} - U_2|_{x_3=\eta}\frac{\partial \eta}{\partial x_2}\,, \tag{17}$$

where x_3 represents the vertical axis and is positive downwards in the left-handed Cartesian coordinate system (x_1, x_2, x_3). The mean velocity components, (U_1, U_2, U_3), dynamic pressure, (P_d), sea surface elevation, (η) and salinity concentration. The velocity and salinity turbulent fluctuations, respectively, (u_1', u_2', u_3') and s'. The reference state variables in the Boussinesq approximation are density ρ_r and salinity S_r. The local density and salinity, ρ and S. Finally, g and f are the gravitational acceleration and the Coriolis parameter.

The mixing processes parametrization in the plume are of prime importance for the dynamical description of the river inputs in the ROFI as well as the plume morphology. Usual 3D numerical models are able to reproduce the global dynamics of stratified plumes except in the interface zone where reduced turbulent fluxes are required. In these cases algebraic models based on Richardson number parametrization are used to fit better with field measurements [23] where the quasi-isotropic two equations (18) and (19) models did not work. Therefore in the numerical model used in this study the algebraic model

closure (20) and (21) is the one developed by [24].

$$-\overline{u_i' u_j'} = \nu_{ti} \frac{\partial U_j}{\partial x_i} \nu_{tj} \frac{\partial U_i}{\partial x_j}\,, \tag{18}$$

$$-\overline{u_i' s'} = K_{ti} \frac{\partial S}{\partial x_j}\,, \tag{19}$$

$$\nu_{tz} = \nu_{tz0}(1 + 10Ri)^{-1/2}, \tag{20}$$

$$K_{tz} = K_{tz0} \left(1 + \frac{10}{3} Ri\right)^{-3/2}, \tag{21}$$

where ν_{ti} and K_{ti} are the kinematic viscosity and the mass diffusivity turbulent coefficients in the x_i-direction and ν_{ti0} and K_{ti0} are the corresponding coefficients in the absence of stratification. Ri is the Richardson number defined as

$$Ri = \frac{(g/\rho_r)\partial\rho/\partial x_3}{(\partial U_1/\partial x_3)^2 + (\partial U_2/\partial x_3)^2}\,. \tag{22}$$

7˙1. *Initial conditions*. – The physical domain where the simulations were carried out was of dimensions of about $50 \times 60\,\mathrm{km}^2$. The 3D Cartesian grid was variable along the three directions with a refined mesh size in the plume (with increments of 500 m horizontally and 0.50 m vertically). At the initial state, salinity and temperature were fixed according to the data collected in the field campaign to account for the seasonal hydrological characteristics. At solid boundaries, impermeable and non-slip conditions were applied while at open sea boundaries, the first spatial derivative was set to zero for salinity and surface elevation, whereas the second derivative was set to zero for velocity. Non-oceanic mesoscale was applied at the open sea boundaries but as the mesoscale circulation follows the shelf break, little interaction with the plume circulation is expected. Thus forcing introduced in the model were fresh-water current at the river mouth and a real bottom bathymetry. The current and salinity inflow profiles were prescribed at the river mouth in order to represent the salt wedge. Despite the numerical model is capable to reproduce the river plume on 3D, in this paper only the superficial dynamic is presented, due mainly to the fact that the experimental conditions do not allow to make this 3D analysis for comparison.

In the numerical model the river flow in the mouth is similar to the described experimental conditions 114, 121, 287 and $635\,\mathrm{m}^3\,\mathrm{s}^{-1}$. The wide mouth was maintained stable in a value of 500 meters, and the fresh-water deep layers were 0.5, 0.5, 1.0 and 2.0 m (reported by [19] from the measured local flows). The corresponding velocity values were 0.45, 0.48, 0.574 and $0.63\,\mathrm{ms}^{-1}$. The reference values of temperature and salinity to all conditions were 21 °C and $37.7\,\mathrm{gkg}^{-1}$. The set of numerical simulations were developed with no wind due to fact that in the experimental model in the rotating table this condition did not apply. The corresponding latitude value to calculate inertial frequencies was 41°N.

8. – Results

8˙1. *Experimental model*

8˙1.1. Induced structures in the water column. The formed structures of the plume by the experimental model under different seasonal conditions reach strongly stabilization

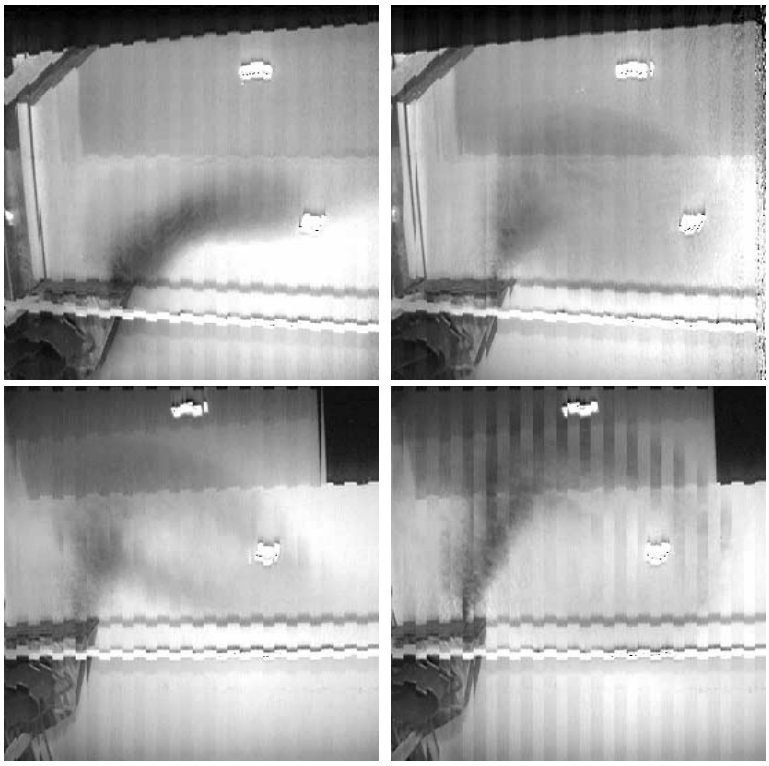

Fig. 6. – Experimental structures from the river plume under 114.33, 121.27, 287.00 and 635.70 $m^3 s^{-1}$ flow conditions at 120 seconds.

on the velocity in the river jet. Figure 6 shows the conditions along 120 seconds—29 days in nature—where all the structures were stable.

In this figure, we can use as a reference the outlet placed in the left side and the Ebro delta shape can be observed in the left bottom corner. The plume structure is outlined by the dye. All the comparative figures will present the following order: Top left Spring conditions, top right Summer conditions, bottom left Fall conditions and bottom right Winter conditions.

For the different conditions, it can be observed that the plumes at 121, 287 and 635 $m^3 s^{-1}$ produced a vortex just in front of the delta. While the plume shaped for the lowest flow is trapped in a big vortex in the south of the delta. Table I shows the vortex

TABLE I. – *Characteristic length from the experimental plume. D = major radius, d = minor radius.*

	Flow ($m^3 s^{-1}$)	D (km)	d (km)
Winter	635.70	104.97	63.41
Fall	287. 00	85.91	66.34
Spring	121.27	75.73	31.40
Summer	114.33	35.83	14.30

Fig. 7. – Superficial induced structures from the flow of $121.27\,\mathrm{m^3\,s^{-1}}$ (Spring conditions) at experimental times of A) 10, B) 30, C) 60, D) 120, E) 180 and F) 240 seconds.

characteristic length in the experiments. The decreasing vortex size that should be related to the Rossby deformation radius was grouped in accordance with the flows in the order Winter, Fall, Spring and Summer.

8˙1.2. Superficial induced structures. The structures observed in the particle tracking experiments, clearly indicated by the particle streaks, which are shown in the four flow conditions developed behaviors in two qualitative different ways. The structures produced by flows 121, 287, $635\,\mathrm{m^3\,s^{-1}}$ and the structures developed by $114\,\mathrm{m^3\,s^{-1}}$. The first type of structures can be summarized in fig. 7 that shows the evolution of the structures at 10, 30, 60, 120, 180 and 240 seconds. The general development was that during

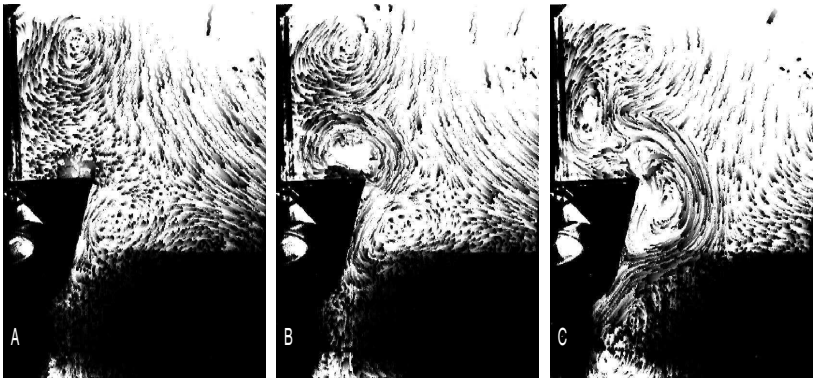

Fig. 8. – Superficial induced structures from the flow of $114.33\,m^3\,s^{-1}$ (Summer conditions) at experimental times of A) 5, B) 30 and C) 120 seconds.

the first stages there was a general circulation forming a large eddy in front of the Ebro delta. The Ebro jet interacted with the general circulation (A), producing a bipolar vortex (B), whose right eddy grew until displaced the general vortex produced by the main tank circulation (C, D). This vortex broke forming a complicated composition of structures (E) and again: the forced vortex, the jet, and the general circulation interact until rise the step B, continuing the sequence.

The second behavior was that presented in the flow of $114\,m^3\,s^{-1}$. Figure 8 shows the general circulation with a large eddy in front of the Ebro delta being also present. The Ebro jet interacted with the general circulation producing a bipolar vortex (A), whose right eddy grew until it broke and formed a littoral current parallel to the Ebro delta coastline (B). Once this vortex was formed, it fed continuously the littoral current towards the south (C). Similar structures such as C were observed since 60 seconds until 600 seconds.

8˙2. *Numerical model.* – The results from the numerical model (sect. **7**) show both qualitative and quantitative values, so that it is possible to study the behavior of a passive tracer as salinity or dye concentration in this case. The salinity values modeled in the surface to the same experimental conditions are shown in fig. 9, where the different distributions from the isolines of salinities 10, 20, 25, 30 and $35\,gkg^{-1}$ were observed.

The plume length derived from the numerical model was calculated as the influenced (ROFI) plume area delimited where the reference salinity ($37.7\,gkg^{-1}$) changed. Figure 10 shows the plume distributions with σ values between 4 and $37.5\,gkg^{-1}$.

The characteristic lengths from the calculated plumes can be observed in table II. If these values are sorted, corresponding with the model flows, they correspond to the seasons: Winter, Spring, Fall and Summer. The modeled superficial velocity fields in fig. 11 show higher velocities near the river mouth and a complex flow, forming a bipolar structure with a northern axis.

8˙2.1. Plume evolution. Under low flow conditions, the numerical simulations were directly compared with the experiments and analyzed for a flow of $114\,m^3\,s^{-1}$ corresponding to the measured Summer conditions [3]. Our aim was to observe the evolution of the $35\,gkg^{-1}$ used as a tracer of the extent of the plume and to follow its behavior in time in a transient corresponding to a sudden increase in the river flow. This comparison

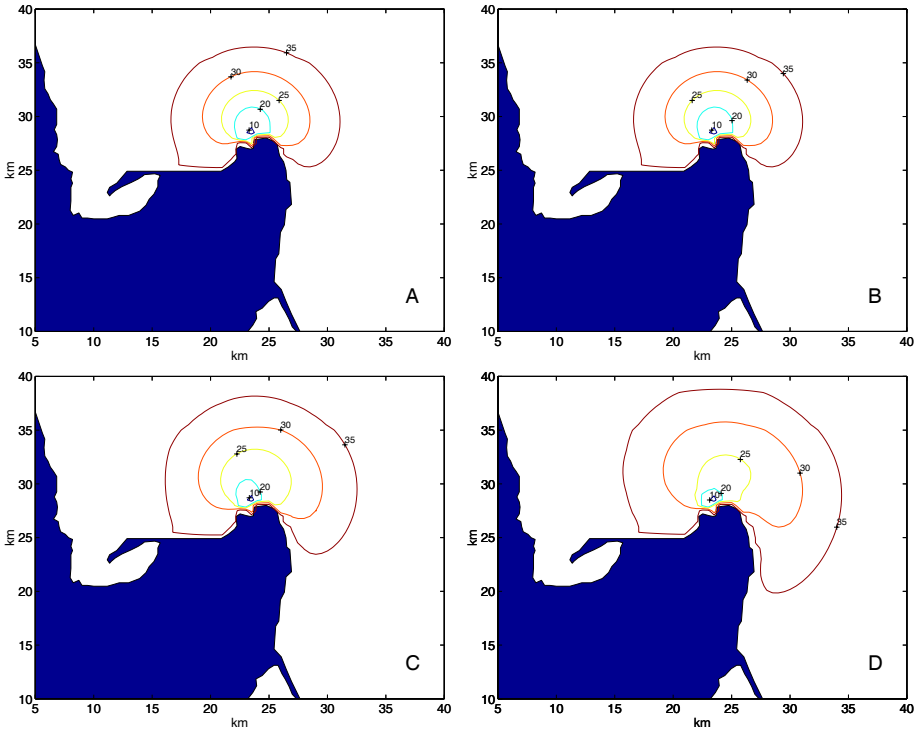

Fig. 9. – Superficial salinity calculated with the numerical model from flows of A) 114.33, B) 121.27, C) 287.00 and D) 635.70 $m^3 s^{-1}$. Experimental time = 33 hours.

between the model and the experiment transients showed that the plume developed during 66 hours following a power law. The growth in time of the average diameters of the plume from the numerical and experimental simulations were, respectively, $D_n = 12t^{1/4}$ and $D_e = 2t^{2/3}$ (fig. 12). In this case, the rate of growth of the plume in the model was significantly lower than in the comparable experiments; on the other hand, the agreement is better for the higher flow rates only in the first 20 hours.

The flow-diameter relationship from both numerical and physical simulations is presented in fig. 13 showing higher final values in the physical simulations for all flows. Two different power laws relating the diameter (D) with the flow (Q) may be used to fit the available flows. The plume diameter-flow function ranged between $D \propto Q^{3/2}$ to $D \propto Q^{1/8}$ for the flow conditions between 114 and 650 $m^3 s^{-1}$.

9. – Discussion

The use of experimental models is important to validate, correct and refine some of the parameters employed in the numerical models. These need further physical interpretations in the case of the environment due to the complex nature of the flows. In addition, it is necessary to perform experimental model validations with natural and or remote observations [25].

9˙1. *Effect of flow variation.* – It is evident that the measured mean flows of 114, 121, 287 and 635 $m^3 s^{-1}$ from Summer, Spring, Fall and Winter conditions can be present

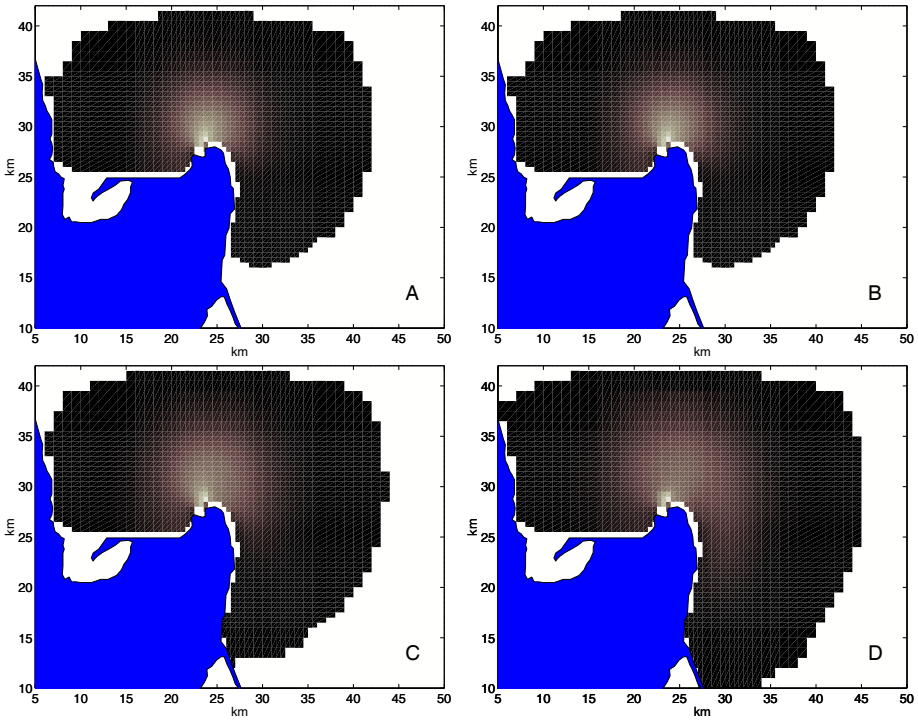

Fig. 10. – Influenced plume area from a time of 33 hours calculated with the numerical model with flow of A) 114.33, B) 121.27, C) 287.00 and D) 635.70 $m^3 s^{-1}$.

anytime in the year, depending on the variable seasonal rain pattern. Furthermore, strong transients are typically associated with strong local precipitation. These particular flows used represent nevertheless typical average seasonal dynamics in the plume and aid to the understanding of the Ebro delta.

It is also evident that the modeled experimental conditions are only present in odd situations when the wind is very low, as this effect could not be modeled in the laboratory experiments.

This work compares the different sources of plume entrainment and allows scale comparison and calibration of the small-scale (or subgrid) mixing between the experimental model and the numerical model following [26] and [8] in the area of the Ebro delta.

TABLE II. – *Characteristic length from the calculated plume in the numerical model. D = major radius, d = minor radius.*

	Flow ($m^3 s^{-1}$)	D (km)	d (km)
Winter	635.70	42.02	26.46
Spring	121.27	35.04	21.98
Fall	287.00	37.08	20.06
Summer	114.33	33.79	31.46

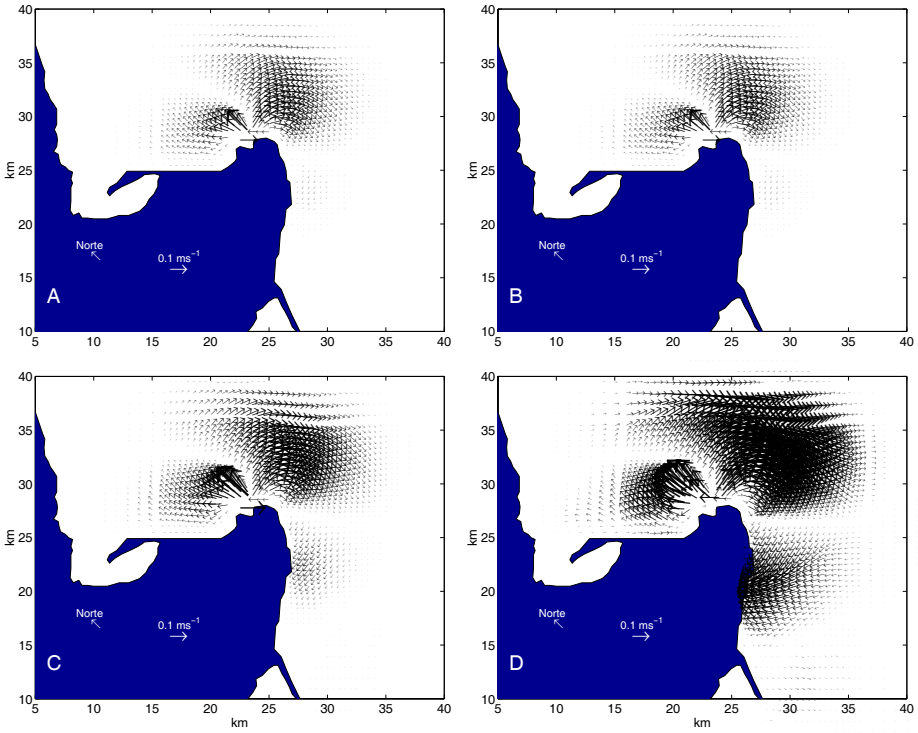

Fig. 11. – Superficial numerical velocity field from flows of A) 114.33, B) 121.27, C) 287.00 and D) 635.70 $m^3 s^{-1}$. Experimental time = 33 hours.

9˙2. *Circulation dynamics.* – The local current dynamics studied in the laboratory model described in sect. **6** were carried out with the Froude-Rossby similarity. So the basic scales are interpreted in accordance with the Froude law and are consistent with the Rossby deformation radius when the time scales are bounded by the planetary vorticity typical time scales f^{-1}. Because the laboratory simulations results can be taken as representative from the natural case in usual conditions we expect that the laboratory scaling and observed structures will be similar to those of the real flow. This is supported also by *in situ* and satellite observations in [27] and [12] where natural structures show length scales of the order of 80 km and a depth of 10 meters from the July 1997 campaign. The authors in ref. [7] emphasize a gyre in the south of the Ebro delta, during February of 1997 consistent with the flow patterns shown in fig. 12 under Spring conditions. In spite of the slope-induced circulation in the experimental area pointed out by [6] and modeled by [10] not all features are reproduced correctly by the experimental model, for example it does not reproduce the change in bathymetry as the natural slope, and it is aimed to investigate transient behavior after an increase of the flow. Although the physical model reproduces reasonably well the range of diameters of the mesoscale plume associated to the end of the continental platform. The numerical results presented only evolve during 66 hours and show a smaller growth rate than the experiments, which could be continued up to 180 h, but then wall effects were significant.

9˙3. *Model differences.* – In the numerical model the effect of wind friction is dominant, and in shallow waters with a strong slope wind friction is much more important than

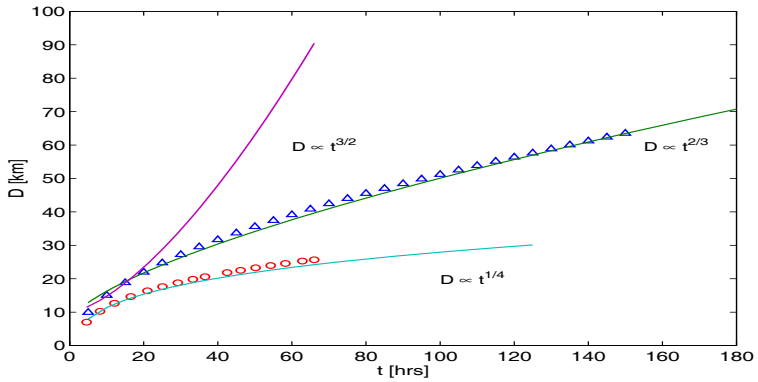

Fig. 12. – Time fits for the diameter values in the river plume with a flow of $114.33\,\mathrm{m}^3\,\mathrm{s}^{-1}$ from the numerical (○) and laboratory (△) simulations.

the bottom friction [28]. This wind-driven environment is present at the superficial plume as shown in the numerical model (see also [23, 21] and [8]). Although bathymetry conditions can also be modeled, these friction inputs have a secondary importance on the characteristic structures within the continental shelf. The main difference between the two models is that numerical model includes the wind input and the effect of the bathymetry while the experimental model was not designed to cope with neither wind nor bathymetry effects.

The numerical plume shows to be very sensitive to the depth of the river layer at the mouth due to a constant mouth width, and different flow values driven by the mean velocity. The main physical effects in the different compared models (laboratory, numerical and natural) are shown in table III.

9˙4. *Plume evolution*. – The growth of the area plume under low flow conditions shown in fig. 12 emphasizes the differences between both numerical and experimental models in time. It can be also observed that the numerical model is more sensitive to

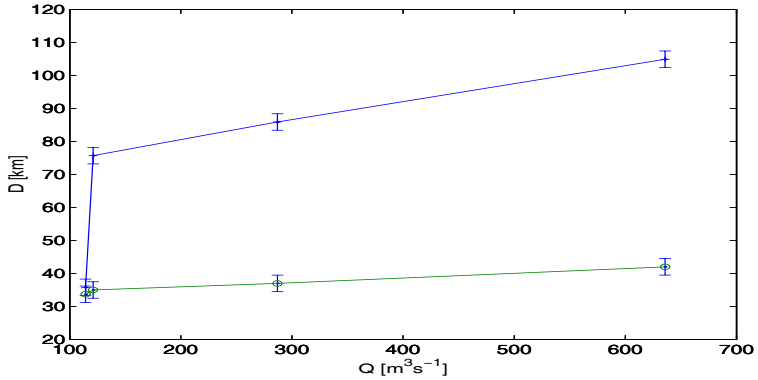

Fig. 13. – Induced length scales from the different flow rates according to numerical model (○) and laboratory experiments (+), during 66 hours.

TABLE III. – *Main physical effects in the numerical, laboratory and natural compared models. Abbreviation key: VI = Very Important; NI = Not Included; MBNI = Modeled But Not Important; MBNVI = Modeled But Not Very Important; NWM = Not Well Modeled; O = Optional and I = Important.*

Model	Effect				
	Wind	Bottom friction	Rotation	River flow	$\Delta\rho$
Numerical	O	MBNI	NWM	VI	I
Laboratory	NI	NI	VI	VI	MBNVI
Natural	VI	VI	VI	I	VI

the boundaries, and the fact that wind was turned off limits strongly the ambient surface diffusivity and thereby the growth of the plume. On the other hand, the experimental model can continue to reproduce the growth of the area (A) due to the external forcing at the Rosby deformation radius. There is an overall agreement on the initial size of the diameters ($D^2 \propto A$) up to about 20 hours of the transients. The strong plume growth reduction observed in the numerical experiments may also be due to the effect of boundaries of the small domain used. While in the experimental model the boundaries seem to be the same as those in nature, controlled seasonally by the rotation and ambient conditions. For the low flows modeled (100 to 120 $\mathrm{m^3\,s^{-1}}$) a power relationship $D \propto Q^{3/2}$ and a different asymptotic relationship ($D \propto Q^{1/8}$) for higher flows are shown in fig. 13.

Previous work with this experimental set presented in [3] showed two main domain areas with an exponential growth of $A \propto t^{1/2}$ in the momentum driven jet domain forming a turbulent front as shown also in the numerical model ($D \propto A^{1/2} \propto t^{1/4}$). Neither the experimental nor the physical models included changes in the continental shelf edge which seem important as pointed in [29] and [10], the results presented in this work nevertheless agree with the structures reported by [27], [7], [6] and [10]. Due to the fact that the large-scale structures are driven mainly by the boundaries they have to be considered in both models. In the experimental model the Rossby deformation scales limited the growth of a coherent plume before the box size was significant, but the forcing of stagnation points without currents in the model offshore conditions may limit the growth of the plume.

9˙5. *Transient processes in the plume.* – The numerical plume with the lowest flow in the mesoscale domain showed in the time series behavior that the river plume area is dependent on the time $A(t)$ marked by the salinity values at 35 $\mathrm{g\,kg^{-1}}$. Considering the area proportional to the square of the mean Lagrangian separation of virtual tracers or the separation variance, the diffusion coefficient can be expressed following Einstein's law as

$$\overline{k}_{h(t)} = \frac{1}{2}\frac{\partial A(t)}{\partial t}\,. \tag{23}$$

While in the experimental plume where the main domain is induced by the large-scale circulation, following (23) the diffusion coefficient will be

$$\overline{k}_{h(t)} = \frac{4}{3}\frac{\partial A(t)}{\partial t}\,. \tag{24}$$

This explains why the transitory processes presented in the plume produce initially up to the mesoscale domain a plume growth following $D \propto t^{1/4}$—like the jet domain in [12]. While the resulting power law for the large-scale domain is $D \propto t^{2/3}$ in the Ebro delta shelf numerical model. The size and positions of the structures by both models are coherent with observations in field campaigns [7, 6, 27]. But for longer times at steady conditions the river plume extension is much smaller than in real non-steady conditions that are described in Richardson's law.

10. – Conclusions

The coherent structures induced by the interaction between the Coriolis force and the flow of the Ebro River in the shelf of the delta shows two kinds of qualitative behavior as a function of the river flow. The lower flow creates a plume that is deflected at the border of a great eddy ($D \simeq 36\,\mathrm{km}$) located in the south of the delta. The medium and higher flows induced the formation of a secondary vortex at the northeast with maximum diameters ($D \simeq 76$, 86 and 105 km), proportional to the flow.

The lower flows forcing vorticity located in the south of the delta induces a southern current. Medium and higher flows produced a vortex in the north of the delta, which interacted with eddies at the east of the delta mostly at the Rossby deformation radius. The interaction produced breaking of the initial coherent structures into several smaller eddies. This action allows the formation of a new vortex at the north of the delta and at that point a new cycle begins. The lengths of the structures as the plume are similar as the induced circulation detected by satellite images [12].

The physical model used in this work shows a much more complex scale dynamics than in the numerical model, set to work at the mesoscale only forced by the river plume and not by winds nor currents.

The length scale structures in the meso-large scale observed in the experimental model are comparable with the structures observed in field, even if the wind component was not considered in this model. The experimental model agrees with the numerical model transient dynamics just during the initial growth of the plume—15–20 km—because the environmental turbulence is underestimated.

The experimental model comparison with the numerical one performed in this work is a very useful test to compare the different sources of local turbulence. So that the overall horizontal diffusivity may be derived from Einstein's relationship applied to marked area growth in time. It is also important to determine in the numerical model information about Rossby deformation scale eddies that effectively affect the boundary conditions and increase the effective ambient diffusivity.

* * *

The laboratory experimentation presented in this work was made thanks to the project HPRI-1999-CT00060 from the EU in the *SINTEF* laboratories in Trondheim, Norway and co-financed by the Generalitat project XT00-0016. The numerical simulation was developed in the *LSEET* of the Université de Toulon et du Var supported by the international mobility program *Erasmus* of the European Union. We thank Prof. T. A. McClimans for his comments during the experimentation at SINTEF, the help from A. Nieys during the stay and the work of E. Pérez during the experiments in Trondheim.

REFERENCES

[1] Simpson J. H., *J. Mar. Syst.*, **12** (1997) 3.
[2] Kourafalou V. H., Lee T. N., Oey L. Y. and Wang J. D., *J. Geophys. Res.*, **101** (1996) 3415.
[3] Carrillo J. A., *Influencia de la turbulencia y de la dinámica de interfaces de densidad sobre organismos planctónicos: Aplicación al estuario del Ebro*. European PhD. Thesis in Marine Sciences, UPC, Barcelona (2002), p. 201.
[4] Cruzado A., Velásquez Z., Pérez M. C., Bahamón N., Grimaldo N. S. and Ridolfi F., *Cont. Shelf Res.*, **22** (2002) 349.
[5] Sierra J. P., Sánchez-Arcilla A., Gonzalez del Río J., Flos J., Movellán E., Mosso C., Martínes R., Rodilla M., Falco. S. and Romero I., *Cont. Shelf Res.*, **22** (2002) 327.
[6] Salat J., García M. A., Cruzado A., Palanques A., Arín L., Gomis D., Guillén J., de León A., Puigdefàbregas J., Sospedra J. and Velásquez Z. R., *Cont. Shelf Res.*, **22** (2002) 327.
[7] Galofré J., Snchez-Arcilla A., Jiménez J. and García M., *Cont. Shelf Res.*, **22** (2002) 379.
[8] Durand N., Fiandrino A., Fraunié P., Ouillon S., Forget P. and Naudin J. J., *Cont. Shelf Res.*, **22** (2002) 267.
[9] Maidana M. A., Naudin J. J., Espino M., García M. A. and Sánchez-Arcilla A., *Cont. Shelf Res.*, **22** (2002) 227.
[10] Xing J. and Davis A. M., *Cont. Shelf Res.*, **22** (2002) 199.
[11] McClimans T. A., *The role of laboratory experiments and models in the study of the sea straits*, in *The Physical Oceanography of the Sea Straits*, edited by Pratt L. J. (Academic Publishers, N. Y.) 1990, pp. 373-388.
[12] Carrillo J. A., Redondo J. M., Sánchez M. A. and Platonov A., *Phys. Chem. Earth*, **26** (2001) 305.
[13] Ibánez C., Pont D. and Prat N., *Limnol. Oceanog.*, **42** (1997) 89.
[14] Ibánez C., Prat N. and Canicio A., *Regul. Rivers*, **12** (1996) 51.
[15] Pritchard D. W., *What is an estuary, physical viewpoint*, in *Estuaries*, edited by Lauf G. H. (American Association for the Advancement of Science, Washington, D.C.) 1967, publ. no. 83.
[16] CHEBRO, Confederación Hidrográfica del Ebro. Banco de Datos `http://chebro.es/banco/`, Ministerio del Medio hambiente (2000) Espanya.
[17] Redondo J. M., Sánchez M. A. and Cantalapiedra I. R., *Dyn. Atm. Oc.*, **23** (1996) 454.
[18] Dalziel S. B., *Dyn. Atmos. Oceans*, **20** (1993) 127.
[19] Carrillo J. A., Redondo J. M., Medina P., González del Rí o J., Moso C. and Movellán E., *Analysis of three-layer mixing conditions in a stratified river estuary*, *EGS 26th General Assembly*, GRA:3 (2001), p. 410.
[20] McClimans T. A., Pietrzack J. D., Hness V., Kliem N., Nielsen J. H. and Johannessen B. O., *Cont. Shelf Res.*, **20** (2000) 941.
[21] Arnau-Chivassa S., Rey V. and Fraunié P., *J. Coast. Res.*, **15** (1999) 61.
[22] Verdier-Bonnet C., Angot P. and Fraunié P., *C. R. Acad. Sci. Sér. II b*, **324** (1997) 229.
[23] Arnau-Chivassa S., *Modélisation d'écoulements côtiers stratifiés présentat des fronts: Application au panache du Rhône*. These pour obtenir le titre de Docteur en Sciences de l'Univers de Toulon et du Var, option Océanographie Physique (1998).
[24] Munk W. H. and Anderson E. A., *J. Mar. Syst.*, **14** (1948) 99.
[25] Platonov A. K., *Aplicación de imágenes de satelité SAR en los estudios de contaminación marina y de dinámica de las aguas del Mediterráneo Noroccidental*. Ph.D. Thesis, UPC (2002), p. 143.
[26] Durand N., *Modélisation numérique tridimiensionnele du penache de l'Ebro*. Ph.D. Thesis, Université de Toulon (2000).

[27] DE LEÓN A. M., *Spatial Objetive Analysis of Oceanographic Variables. An Application to the Ebro Delta Shelf-Slope Domain (North-western Mediterranean)*. Memoria para optar al titulo de Doctor en Ciencias del Mar, CSIC. ICM. UPC (2002), p. 216.
[28] LI S. and MCCLIMANS T. A., *Cont. Shelf Res.*, **18** (1998) 457.
[29] GJEVIK B., MOE H. and OMMUNDSEN A., *Cont. Shelf Res.*, **22** (2002) 173.